Inclusive strange-particle production in single-vee events in 200-GeV/c $\pi^- N$ interactions

S. Mikocki,[a] J. R. Ficenec, S. Torres,[b] and W. P. Trower
Virginia Polytechnic Institute and State University, Blacksburg, Virginia 24061

T. Y. Chen,[c] E. W. Jenkins, K-W. Lai, J. LeBritton,[d] Y. C. Lin,[e] and A. E. Pifer
University of Arizona, Tucson, Arizona 85721

H. C. Fenker and D. R. Green
Fermilab, Batavia, Illinois 60510

J. R. Albright, J. H. Goldman, S. L. Hagopian, J. E. Lannutti, and J. E. Piper[f]
Florida State University, Tallahassee, Florida 32306

C. C. Chang,[g] T. C. Davis,[h] R. N. Diamond,[i] K. J. Johnson,[j] and J. A. Poirier
University of Notre Dame, Notre Dame, Indiana 46556

A. Napier and J. Schneps
Tufts University, Medford, Massachusetts 02155

J. M. Marraffino, J. W. Waters, M. S. Webster, and E. G. H. Williams[k]
Vanderbilt University, Nashville, Tennessee 37235

(Received 13 September 1985)

For the reaction $\pi^- N \to V^0 X$, where V^0 is a K_s^0, Λ, and $\bar{\Lambda}$ and X are charged particles, we measured the transverse- and longitudinal-momentum distributions, and inclusive cross sections for the V^0 and for $K^{*\pm}(892)$, $\Sigma^{\pm}(1385)$, and $\Xi^{\pm}(1321)$. We compare our results with predictions of quark-counting rules, and conclude that valence quarks play an important role in strange-particle production.

INTRODUCTION

Inclusive strange-particle production is of intrinsic interest as a probe of the strong interaction.[1,2] In high-energy π-nucleon interactions strange-particle production requires that an additional quantum-number pair be created whose dynamics provide information about the strong interactions. Neutral strange particles decaying to charged pairs provide an excellent experimental signature for the production of strangeness over a large range of longitudinal momentum (X_F). Further, strangeness can be a signature of charm production,[3] a subject of current interest.[4] Finally, new narrow resonances can be probed using a definite final state such as e^+e^- or $\mu^+\mu^-$ ($\rho,\omega,\phi,J/\psi,\Upsilon$) whose spin-parity is restricted to $J^P=1^-$. Different spin-parity states decay to two neutral strange particles, specifically $K_S^0 K_S^0$ and $\Lambda\bar{\Lambda}$.

The valence-quark content of an incident beam and target is reflected in the quantum numbers and momentum distribution in the fragmentation region.[1,2] Less is known about the role of these valence quarks in strange-particle production, especially at high energies. In multiparticle production in soft collisions the X_F distribution of fast hadrons with low transverse momentum (P_T) depends on the quark-parton models used.[1] The so-called quark-counting rules (QCR's) form one class of such models. For the inclusive distributions observed in fragmentation processes as $X_F \to 1$, QCR's predict the n of $d\sigma/dX_F = A(1-X_F)^n$, where n is interpreted as the number of spectator quarks involved. The exponent n differs if quark or gluon exchange is dominant or if the sea

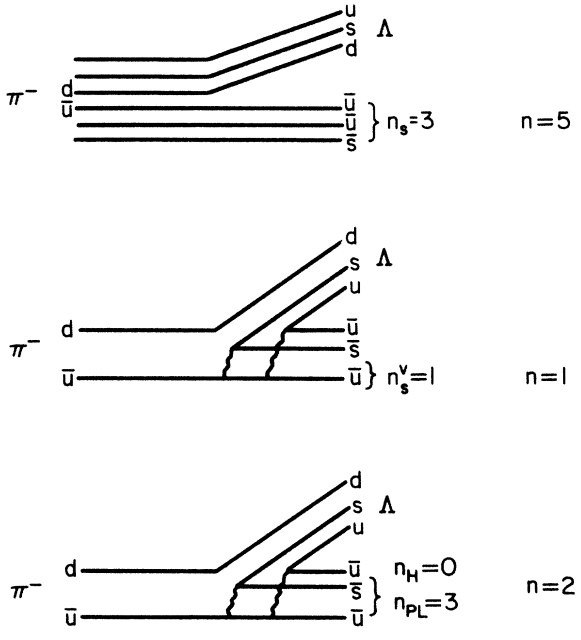

FIG. 1. Fragmentation diagrams for $\pi^- \to \Lambda$.

quarks are among the spectators, and depends on the details of how all this is accomplished.

Initially QCR's predicted $n=2n_s-1$, where n_s is the least number of spectator valence and sea quarks from the beam hadron. This prediction disagrees with experiment. Counting only valence quarks as spectators, n_s^v, n has been predicted as $2n_s^v-1$. This prediction, although more successful, does not predict the observed baryon spectra steepness in meson fragmentation. QCR's, using lowest-order quantum chromodynamics (QCD), predict[2] $n=2n_H+n_{\rm PL}-1$, where n_H is the number of initial hadron spectator quarks and $n_{\rm PL}$ is the number of spectators emerging from pointlike bremsstrahlung interactions. These three QCR diagrams for $\pi^-\to\Lambda$ are shown in Fig. 1.

Some results from the Fermilab Multiparticle Spectrometer (FMPS) experiment E580 have been reported previously.[5–9] Here we report the analysis of events with only one reconstructed V^0. We first describe the FMPS, trigger, and data analysis. We then report the production of strange particles [K_S^0, Λ, $\bar{\Lambda}$, Ξ^-, $\bar{\Xi}^+$] and resonances [$K^{*\pm}(892)$, $\Sigma^{\pm}(1385)$], which we compare with QCR's.

THE APPARATUS

Experiment E580 triggered on reactions $\pi^-N\to V^0V^0X$ where V^0 was a K_S^0, Λ, or $\bar{\Lambda}$ while X were charged particles. The experiment was carried out with the FMPS, shown in Fig. 2, in the 200-GeV/c π^- M6W beam line. Not shown upstream of the target are two in-beam coincidence counters and an anticoincidence hole counter which defined the beam, and three proportional-wire-chamber (PWC) modules (BA1–3) which provided beam direction.

The active target was 20 individual (3.172 ± 0.003 cm^2 by 0.621 ± 0.006 cm) plastic scintillators (Pilot-B with $\rho\sim1.032$ g/cm^3). Each counter, wrapped in aluminum foil and heat shrink tubing, had a center-to-center spacing of 1.29 cm. For each trigger the pulse height of each counter was recorded.

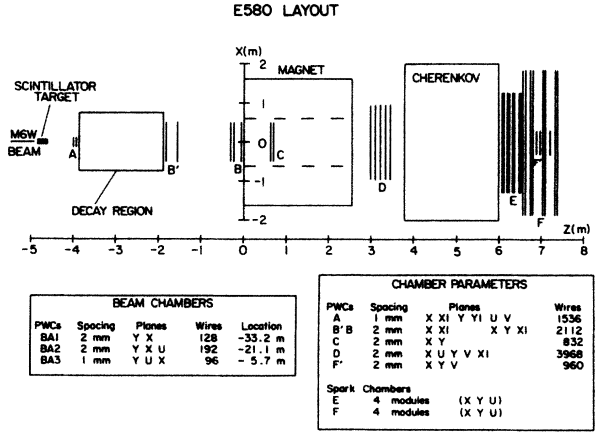

FIG. 2. The experimental apparatus.

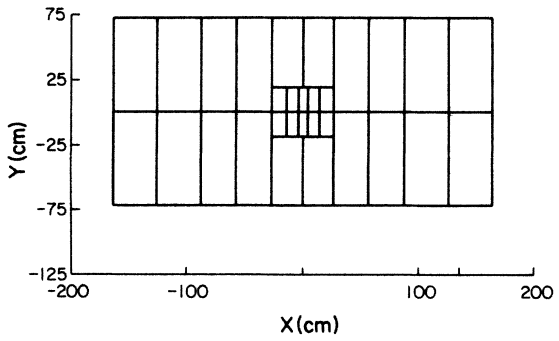

FIG. 3. Cherenkov mirror plane segmentation.

Directly downstream of the target was the six-PWC plane A station with two $x(0°)$, two y (90°), and a u-v pair inclined at $\pm45°$ to vertical. Downstream of the A station was a decay region, filled with helium gas to reduce interactions, where neutral strange particles decayed into charged tracks (V^0). Next the five-PWC plane B'-B station was in front of the spectrometer magnet. The superconducting ferrite magnet of aperature $122(x)\times72(y)\times256(z)$ cm produced a 16.9-kG centrally homogeneous field at a maximum excitation of 180 A and imparted a 697-MeV/c P_T change to each charged particle. Mounted directly upstream of the magnet pole piece was the C station with two PWC planes.

Downstream of the magnet was the five-PWC plane D station whose $u-v$ pair was inclined at $\pm15°$ to the vertical. Following was a nitrogen-filled, atmospheric-pressure Cherenkov counter with 30 cells. Figure 3 shows the Cherenkov mirror segmentation while Table I summarizes its parameters. Next were eight large magnetostrictive spark-chamber modules, the E and F stations, constructed in two-gap units with stretched aluminum wire electrodes. Each unit of the E and F chamber modules had one gap with x electrodes and one formed with wires tilted at $\tan\theta=\pm0.1$ to the vertical. Each module with three magnetostrictive planes x, y, and either u or v had a sensitive area of $\sim2.4\times1.2m$ (E) or $\sim3.6\times1.8m$(F). Interspaced in the beam region of the F station were the F' station PWC's with a x-y pair and one v at 45°.

TABLE I. Cherenkov C_B physical characteristics.

Dimensions	$226\times122\times330$ cm^3
Mirror area	322×142 cm^2
NTP gas	N_2
Refractive index	1.0003
Radiator length	177 cm
Cone radius ($\beta=1$)	4 cm
Number of mirrors	30
Mirror to target distance	8.7 m
Pion threshold	5.7 GeV/c
Kaon threshold	20.0 GeV/c
Proton threshold	38.8 GeV/c

THE TRIGGER

A defined beam particle and the absence of a signal in a small scintillation counter placed in the deflected beam line after the Cherenkov counter was an interaction. The trigger then counted the track hit clusters in A_u and A_v before, and B_x', $B_{x'}'$, C_x, C_y, D_x, D_y, and $D_{x'}$ after, the decay volume. The V^0V^0 trigger required a cluster multiplicity increase of 4 ± 1 in the decay volume; multiplicity in at least two C and D planes equal to that measured in the B' station; and a primary cluster multiplicity measured before the decay volume of ≤ 5. Up to three consecutive wire hits defined a cluster. Further, each target counter pulse height was summed to determine if the interaction had taken place there. Although the experiment was designed to trigger on V^0V^0 events, true V^0 events could satisfy the V^0V^0 trigger requirements if an interaction produced tracks between the A and B' stations or if closely spaced multiple tracks formed one cluster in the A station, but not in the B station. Using different models for the trigger, we estimated that the trigger for V^0 events was ~ 4 times lower than for V^0V^0 events.

THE DATA

The average beam intensity was $\sim 6\times 10^5\pi^-$ in a 1-s spill over a 400-h run which resulted in the total of $1.2\times 10^{10}\pi^-$ giving $1.2\times 10^6 V^0V^0$ triggers. An additional 3×10^5 triggers of noninteracting beam, elastic scattering (1π), diffractive (3π's), and $V^0\pi$ events were taken for diagnostic purposes and to verify the mass and momentum scales. The diagnostic $V^0\pi$ events are not included in the analysis reported here.

All triggers were passed through a pattern-recognition program TEARS. A noninteracting beam was used for momentum calibration, alignment, and program tune-up. TEARS found straight track segments upstream and downstream of the magnet which were matched at the magnet midplane. Upstream segments which did not have hits in the A station were candidates for V^0 decay legs. Loose cuts were made on the V^0 mass and on the vertex in the decay volume.

Next, a global three-dimensional spline fit was made using a detailed magnetic field map to obtain momentum and angles for each track. Each V^0 was tested with three hypotheses: K_S^0, Λ, and $\bar{\Lambda}$. For the best hypothesis the K_S^0 mass distribution had a full width at half maximum (FWHM) of 14 MeV/c^2 while the Λ and $\bar{\Lambda}$ distributions had a FWHM of 5 MeV/c^2. Finally, track parameters were varied in fits constrained to the V^0 mass and decay vertex location, requiring the fit probability $\geq 10^{-5}$. Of the surviving $\sim 70\,500 V^0V^0$ events, 62% were $K_S^0K_S^0$, 16% $K_S^0\Lambda$, 13% $K_S^0\bar{\Lambda}$, 8% $\Lambda\bar{\Lambda}$, and 1% $\Lambda\Lambda$ or $\bar{\Lambda}\bar{\Lambda}$. Of the $\sim 25\%$ of the $\sim 230\,000$ events where a single V^0 was reconstructed 76% were K_S^0, 13% Λ, and 11% $\bar{\Lambda}$. Ambiguities between the K_S^0 and the Λ or the $\bar{\Lambda}$ mass hypotheses exist over a small range of V^0 decay angles, and they are usually resolved as K_S^0. The frequency of incorrect assignment is measured from decay angular distributions to be a few percent in the $K_S^0\Lambda$ and $K_S^0\bar{\Lambda}$ events, but is not apparent in single or double K_S^0 events. Therefore we estimate the V^0 mass ambiguities to be less than 1% in the V^0 events.

The primary interaction vertex was found by two methods. In the first, all tracks, excluding beam and V^0 tracks, were fitted to a point, requiring the χ^2 per degree of freedom, χ^2/DF, ≥ 30. The poorest fitting track was deleted and the fit repeated. The vertex had to lie within 5σ of the target boundaries. In the second method, the target analog-to-digital converters (ADC's) were examined for abrupt pulse-height increases, with up to three allowed. One such increase unambigiously gave the interaction vertex z coordinate. Using the beam PWC's, the x and y track coordinates of the z interaction point were computed. When both methods gave a solution and the difference in their z coordinates was greater than twice their summed z-coordinate errors, the direct track vertex was rejected, because it is a less direct measurement and because it often is a result of secondary interactions. Otherwise, a weighted average of the two solutions was taken.

We then made cuts to eliminate false tracks found in pattern recognition as well as secondary interactions. We required that the primary vertex be $\leq 5\sigma$ from the target boundaries and that the total visible momentum (V^0 plus charged tracks) $\leq$ 230 GeV/c or we discarded the event. The V^0 had to point to the primary vertex ($\chi^2<20$) and the decay vertex had to be within 3σ of the decay region. Since the pattern-recognition program occasionally found, by using several common chamber cluster hits, two nearly identical track segments upstream of the magnet, we cut on the slope and intercept differences ($\Delta\theta$ and Δb) of the upstream tracks. The difference in slopes of the V^0 legs in the x-z (y-z) view had to be $\Delta\theta_x \geq 0.5$ ($\Delta\theta_y \geq 0.15$) mrad and the leg intercept difference had to be $\Delta b_x \geq 0.15$ ($\Delta b_y \geq 0.15$) cm or the V^0 was discarded. Each charged track was required to (1) have momentum ≤ 210 GeV/c, (2) have a χ^2 relative to the vertex of ≤ 35, and (3) possess slope or intercept differences from V^0 legs of $\Delta\theta_x \geq 0.9$ ($\Delta\theta_y \geq 0.4$) mrad or $\Delta b_x \geq 0.25$ ($\Delta b_y \geq 0.15$) cm, or the track would be discarded. Two primary tracks with slope and intercept differences $\Delta\theta_x \leq 0.4$ ($\Delta\theta_y \leq 0.25$) mrad and $\Delta b_x \leq 0.20$ ($\Delta b_y \leq 0.12$) cm resulted in one of the tracks being discarded. These cuts reduced the event sample to 25 565 K_S^0, 3999 Λ, and 3041 $\bar{\Lambda}$.

We study particle production by examining invariant-mass distributions for given decay modes and fitting the $X_F(dN/dX_F)$ or $dN/dX_F = A(1-X_F)^n$ and $(dN/dP_T{}^2) = B\exp(-bP_T{}^2)$ distributions. The backgrounds for these distributions are obtained from mass sidebands of the system under study. Only the X_F distributions are acceptance corrected using Monte Carlo–generated events for a given reaction with a flat X_F distribution and $P_T{}^2$ distribution with $b=2.5$ (GeV)/$c)^{-2}$ unless noted otherwise. These events were propagated through the FMPS using computer codes that take into account the detector geometry and the restricted V^0 decay region. In performing the fits, the χ^2 contribution of each histogram bin is based on the difference between the number of events in the bin and the integral of the fitted function over that bin interval. The fits were obtained using a χ^2-minimizing program (MINUIT) whose fit-parameter error was determined by an increase in χ^2 by one.

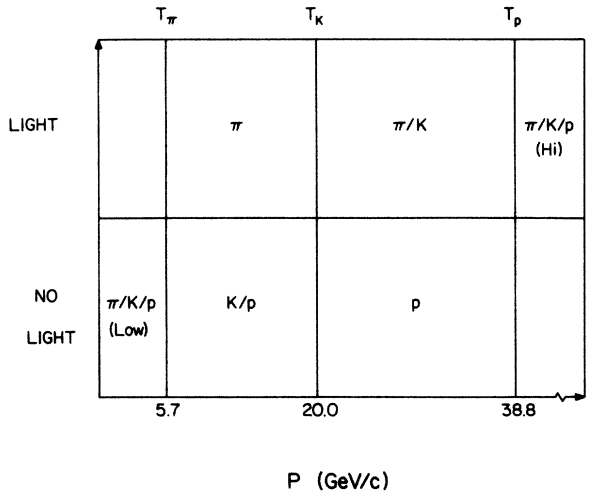

FIG. 4. Particle-identification momenta regions.

PARTICLE IDENTIFICATION

Charged-particle identification was made using the Cherenkov counter data with an identification algorithm[10] since the pion, kaon, and proton momentum thresholds define four distinct momentum region, as seen in Fig. 4. Tracks with a momentum below the pion Cherenkov threshold, which however still have the associated Cherenkov light, could be electrons or they could result from tracking or identification algorithm inefficiencies. Above the momentum for which protons should emit light, the small fraction where we observe no light we attribute to detector or algorithm inefficiency or to spurious tracks. The interpretation of the other regions is found in Fig. 4. We found an average identification inefficiency of $\sim 20\%$ per particle by comparing Cherenkov assignments with the V^0 leg masses determined by the kinematic fits. Ambiguous tracks with a π/K interpretation we call pions, and particles with a momentum between 20.0 and 38.8 GeV/c which gave no light we call protons. For the analysis reported here particle identification was not used and all direct charged tracks were assumed to be pions.

K_S^0 AND K^* (892) PRODUCTION

In Fig. 5 we plot the K_S^0 X_F distribution, where a fit over $0.2 \leq X_F < 0.8$ gives $n = 1.7 \pm 0.1$ with $\chi^2/\mathrm{DF} = 10/13$. The QCR predict an $A(1-X_F)^3 + B(1-X^F)^1$ dependence; this fit yields $A/B = 1.7 \pm 0.1$ with $\chi^2/DF = 15/13$.

The K_S^0 $P_T{}^2$ distribution, shown in Fig. 6, is fit best by a sum of two exponentials with slopes 2.1 ± 0.3 and 5.0 ± 0.5 $(\mathrm{GeV}/c)^{-2}$ while restricted X_F regions fit well to a single exponential with 2.6 ± 0.1 $(0.3 \leq X_F < 0.5)$, 2.7 ± 0.1 $(0.5 \leq X_F < 0.7)$, and 3.1 ± 0.3 $(\mathrm{GeV}/c)^{-2}$ $(0.7 \leq X_F < 0.1)$ showing that $P_T{}^2$ increases slightly with X_F. Correcting for acceptance yields 2.5, 2.6, and 2.9, respectively, over the X_F range.

The fits to the $K_S^0\pi$ invariant-mass distribution, for

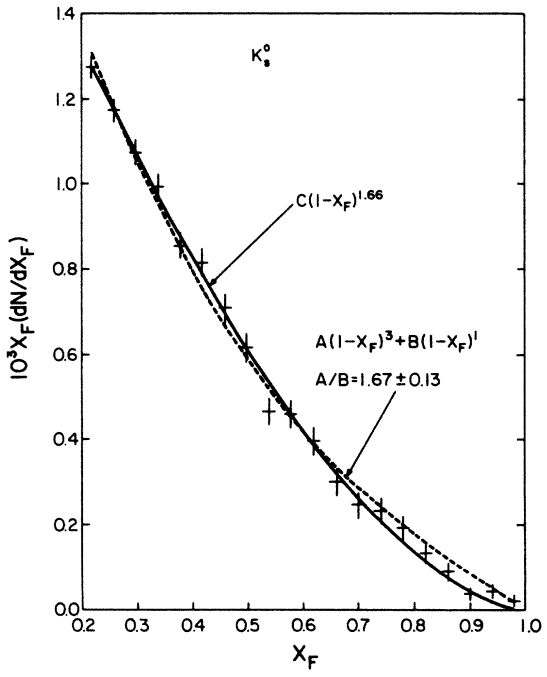

FIG. 5. The K_S^0 X_F distribution.

$X_F > 0$ and all $P_T{}^2$, are shown in Fig. 7. Although there is more $K^{*-}(892)$ than $K^{*+}(892)$ the K^* fraction in $K_S^0\pi$ is consistent for both charge states. We use a P-wave Breit-Wigner[6] for the $K^*(892)$ and a background of

$$A(M-m_0)^B \exp[-C(M-m_0)-D(M-m_0)^2] ,$$

where M is the $K\pi$ mass, m_0 the threshold mass, and A,

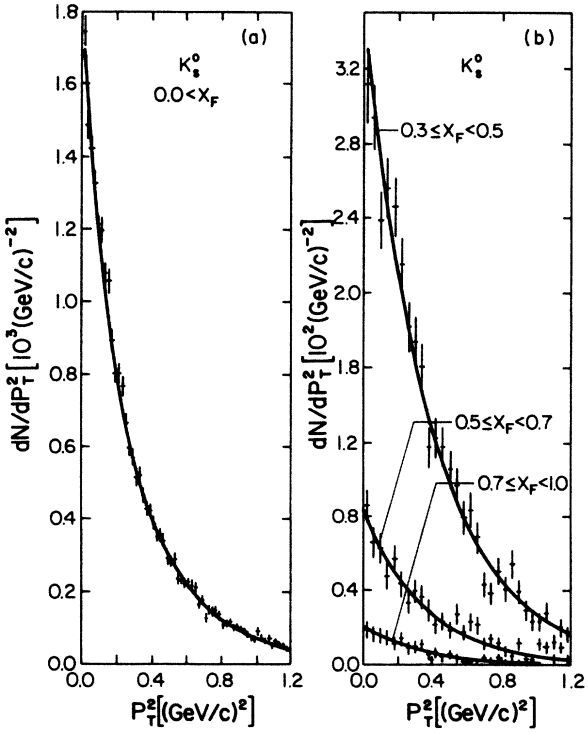

FIG. 6. The K_S^0 $P_T{}^2$ distributions.

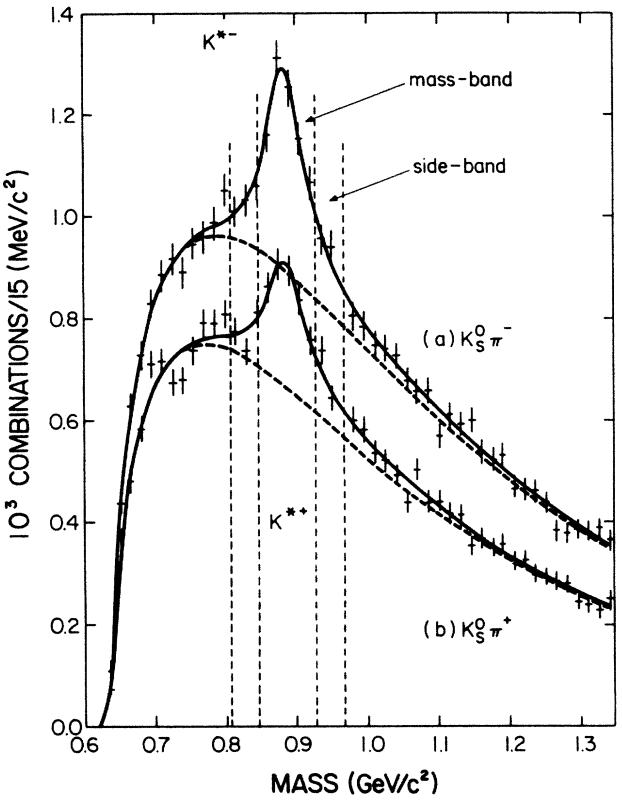

FIG. 7. Mass spectra for $K^0_S\pi^{\pm}$.

B, C, and D are fit parameters. The fitted mass (MeV/c^2), full width at half- maximum (MeV/c^2), and number of events with χ^2/DF, all summarized in Table II, are 888±2, 64±8, 2706±313 with 31/41 for the K^{*-} and 889±3, 70±12, 1813±309 with 51/41 for the K^{*+}. The K^{*0} X_F distribution, shown in Fig. 8, gives $n=0.9\pm0.2$ with $\chi^2/\mathrm{DF}=3/2$ for K^{*-} and 1.9 ± 0.4 with $\chi^2/\mathrm{DF}=1/2$ for the K^{*+}. The X_F ratio, which is acceptance independent, gives $n=1.1\pm0.4$ and $R(X_F=0)=1.0\pm0.2$ with $\chi^2/\mathrm{DF}=2/3$.

The K^* $P_T{}^2$-dependence fit, shown in Fig. 9, gives $b=2.7\pm0.3$ for K^{*-} and 2.5 ± 0.3 (GeV/c)$^{-2}$ for K^{*+} for $0\le P_T{}^2\le 1.2$ (GeV/c)^2 with $\chi^2/\mathrm{DF}=13/4$ and 11/4, respectively. The ratio of K^* to K^0_S is 0.071 ± 0.012 and 0.106 ± 0.012 for the K^{*+} and K^{*-}, respectively. If K^{*0} and $\overline{K}{}^{*0}$ production is equal to K^{*+} and K^{*-}, then our $R(K^*/K^0_S)\sim0.35$ is consistent with bubble-chamber experiments.[11]

Λ, Ξ(1321) AND Σ(1385) PRODUCTION

In Fig. 10 we plot the Λ and $\overline{\Lambda}$ X_F distributions which, when fit for $0.15\le X_F<0.8$, gives $n=2.0\pm0.1$ with $\chi^2/\mathrm{DF}=7/11$ for Λ and 2.0 ± 0.1 with $\chi^2/\mathrm{DF}=12/11$ for $\overline{\Lambda}$. The $R(\overline{\Lambda}/\Lambda)\sim0.6$ at $X_F\sim0$ indicates target proton fragmentation. For $0.1\le X_F<0.65$, $R(\overline{\Lambda}/\Lambda)\sim0.8$, and for $X_F\ge0.65$ $R(\overline{\Lambda}/\Lambda)$ increases above 1. This behavior was also seen in the $K^0_S\Lambda/K^0_S\overline{\Lambda}$ data sample.[7]

A single exponential fit to the $P_T{}^2$ distributions, shown in Fig. 11, for $X_F>0$ gives $b=2.5\pm0.1$ (GeV/c)$^{-2}$ with

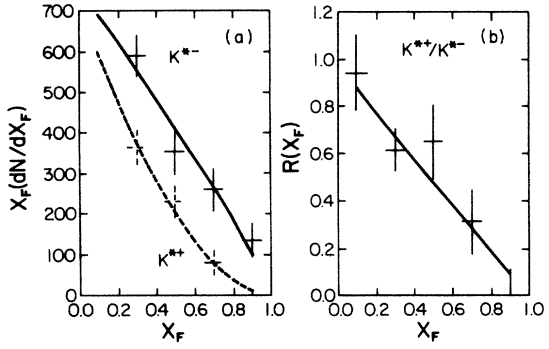

FIG. 8. The X_F distributions for (a) K^{*-} and K^{*+} and (b) $R(K^{*+}/K^{*-})$.

$\chi^2/\mathrm{DF}=19/22$ for Λ and 2.6 ± 0.1 (GeV/c)$^{-2}$ with $\chi^2/\mathrm{DF}=30/22$ for $\overline{\Lambda}$. For $0.3\le X_F<0.5$ and $0.5\le X_F<0.7$, the slopes are 2.6 ± 0.2 and 2.3 ± 0.3 (GeV/c)$^{-2}$ for Λ, and 2.4 ± 0.2 and 2.1 ± 0.4 (GeV/c)$^{-2}$ for $\overline{\Lambda}$.

The Ξ(1321), present in $\Lambda\pi^-$ and $\overline{\Lambda}\pi^+$ distributions, is shown in Fig. 12, where a fit to a Gaussian resonance with standard deviation σ and a quadratic background, $A(M-m_0)+B(M-m_0)^2$. The results, summarized in Table II, are 48 ± 10 Ξ^- events with M and σ of 1322.1 ± 0.3 and 1.2 ± 0.3 MeV/c^2 and with $\chi^2/\mathrm{DF}=76/75$, and 33 ± 10 $\overline{\Xi}{}^+$ events with M and σ of 1322.2 ± 0.4 and 1.3 ± 0.5 MeV/c^2 and with $\chi^2/\mathrm{DF}=101/75$. A fit to the combined distribution gives 72 ± 15 events with M and σ of 1322.2 ± 0.3 and 1.1 ± 0.3 MeV/c^2 and with $\chi^2/\mathrm{DF}=75/75$. Our mass is slightly

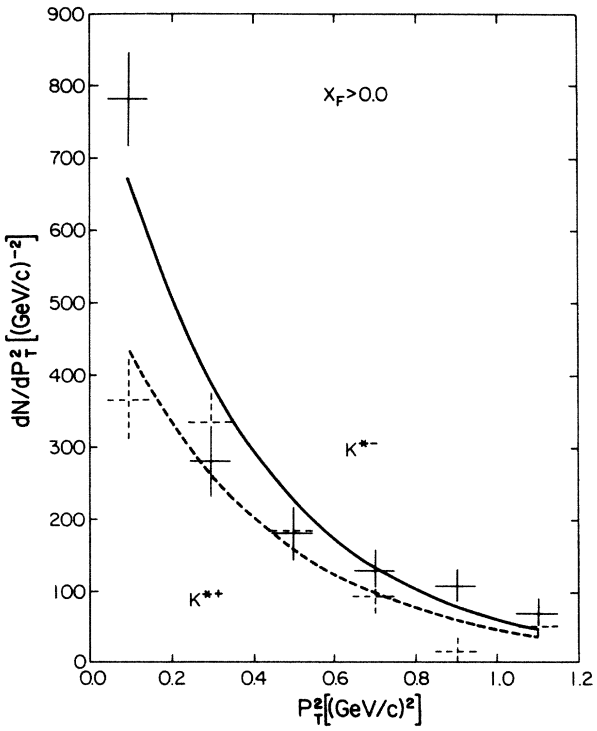

FIG. 9. The $P_T{}^2$ distribution for K^{*-} and K^{*+}.

TABLE II. Fits to mass distributions. Parameters without errors were fixed in the fit.

State	Mass (MeV/c^2)	Γ or $\sigma(\Xi)$ (MeV/c^2)	Events	χ^2/DF
$K^{*-}(892)$	888±2	64±8	2706±313	31/41
$K^{*+}(892)$	889±3	70±12	1813±309	51/41
$\Xi^-(1321)$	1322.1±0.3	1.2±0.3	48±10	76/75
$\Xi^+(1321)$	1322.2±0.4	1.3±0.5	33±10	101/75
$\Xi^- + \Xi^+$	1322.2±0.3	1.1±0.3	72±15	75/75
$\Sigma^-(1385)$	1387	45	219±50	53/44
$\Sigma^+(1385)$	1382	40	154±46	58/45
$\bar{\Sigma}^-(1385)$	1382	40	84±40	56/45
$\bar{\Sigma}^+(1385)$	1387	45	64±42	45/44

higher than the accepted[3] 1321.52±0.13 MeV/c^2 and our width is consistent with our mass resolution of 1.5 MeV/c^2 at the Ξ mass.

The X_F distributions, shown in Figs. 13(a) and 13(b), give $n=2.2\pm2.0$ for Ξ^- and 8.4 ± 9.0 for $\bar{\Xi}^+$. The $P_T{}^2$ distributions, shown in Figs. 13(c) and 13(d), give $b=2.8\pm1.1$ and 2.1 ± 1.1 (GeV/c)$^{-2}$, respectively, for Ξ^- and $\bar{\Xi}^+$. In Fig. 14 we plot $\Lambda\pi^-$ and $\bar{\Lambda}\pi^+$ mass combinations and observe the $\Xi(1321)$ and $\Sigma(1385)$. In Fig. 15, $\Sigma^+(1385)$ is seen in $\Lambda\pi^+$ but the $\bar{\Sigma}^-(1385)$ is only marginally present in $\bar{\Lambda}\pi^-$. We fit a Gaussian to the $\Xi(1321)$, a Breit-Wigner to the $\Sigma(1385)$ and $A(M-m_0)^B\exp[-C(M-m_0)^D]$ to the background, with masses fixed at the accepted values[3]. The $\Xi(1321)$ widths were taken from the previous fits and the accepted $\Sigma(1385)$ widths were increased by 5 MeV/c^2 to account for our mass resolution $\sigma=2$ MeV/c^2 at the Σ mass. The results, summarized in Table II, are 219 ± 50 $\Sigma^-(1385)$, 154 ± 46 $\Sigma^+(1385)$, 84 ± 40 $\bar{\Sigma}^-(1385)$, and 64 ± 42 $\bar{\Sigma}^+(1385)$ events with a strange antibaryon: baryon ratio of $\sim0.4{:}1$. Fits to the X_F and $P_T{}^2$ distributions, seen in Fig. 16, for the more statistically significant $\Sigma^-(1385)$ and $\Sigma^+(1385)$, give $n=1.4\pm0.4$ with $\chi^2/\mathrm{DF}=0.04/3$ and $b=3.9\pm2.4$ (GeV/c)$^{-2}$ with $\chi^2/\mathrm{DF}=0.7/4$ for $\Sigma^-(1385)$, and $n=3.8\pm2.2$ with 0.07/2 and $b=2.9\pm1.4$ with 1/4 for $\Sigma^+(1385)$.

COMPARISON WITH QCR'S AND OTHER DATA

In Table III we summarize our fits to X_F distributions together with the predictions.[2] Our experimental n values, though systematically lower, are consistent with QCR's except for K^{*+}. Since particles produced without a valence beam quark have a steeper X_F distribution than

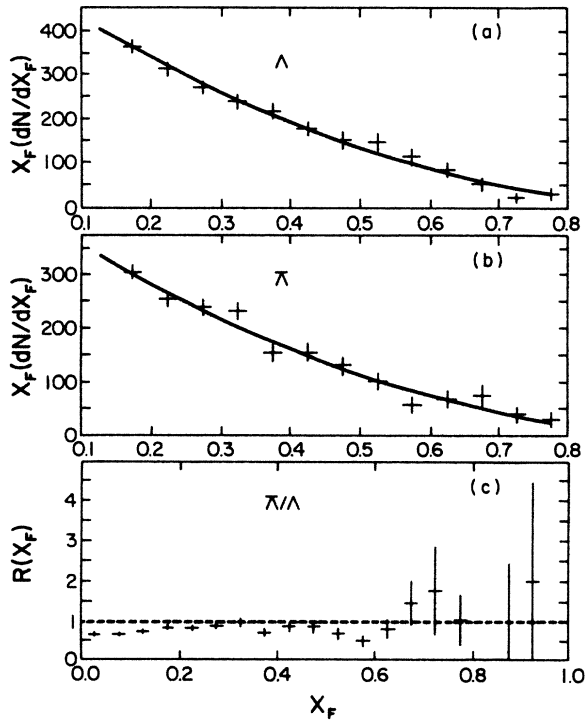

FIG. 10. The X_F distributions for (a) Λ, (b) $\bar{\Lambda}$, and (c) $R(\bar{\Lambda}/\Lambda)$.

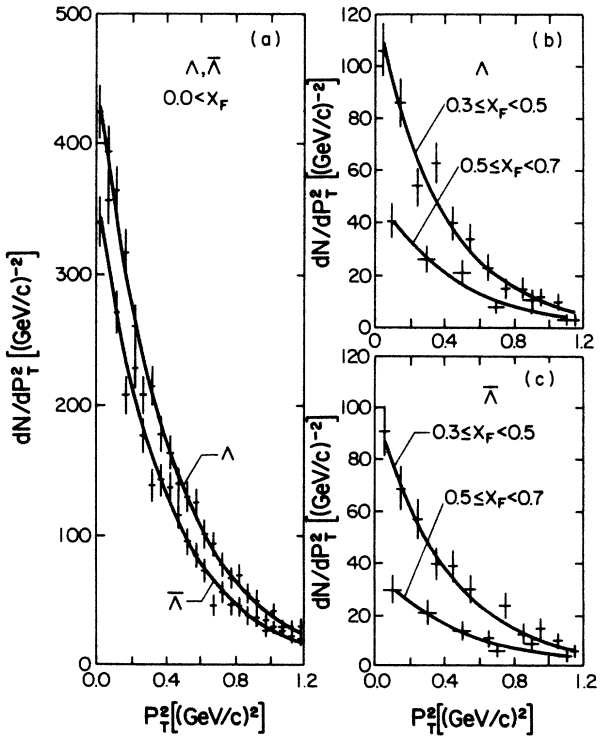

FIG. 11. The $P_T{}^2$ distribution for (a) $\bar{\Lambda}$ and Λ, (b) Λ, and (c) $\bar{\Lambda}$.

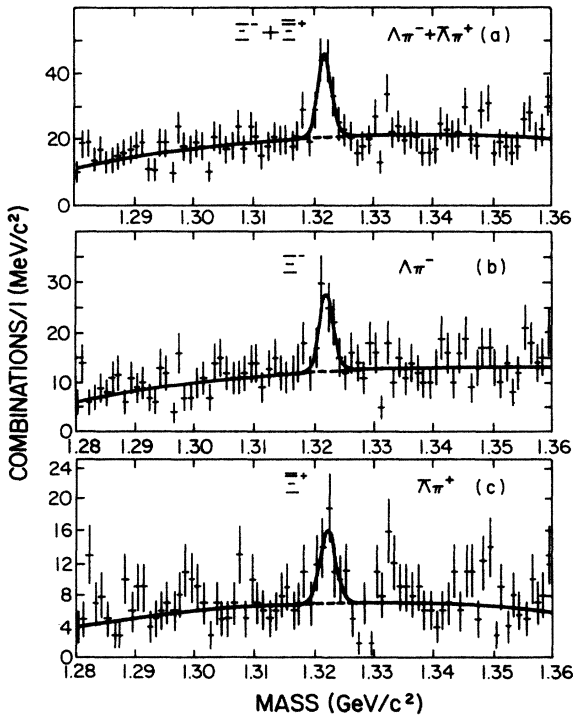

FIG. 12. Mass spectra of Ξ(1321) region for (a) $\Lambda\pi^{\pm}$, (b) $\Lambda\pi^{-}$, and (c) $\bar{\Lambda}\pi^{+}$.

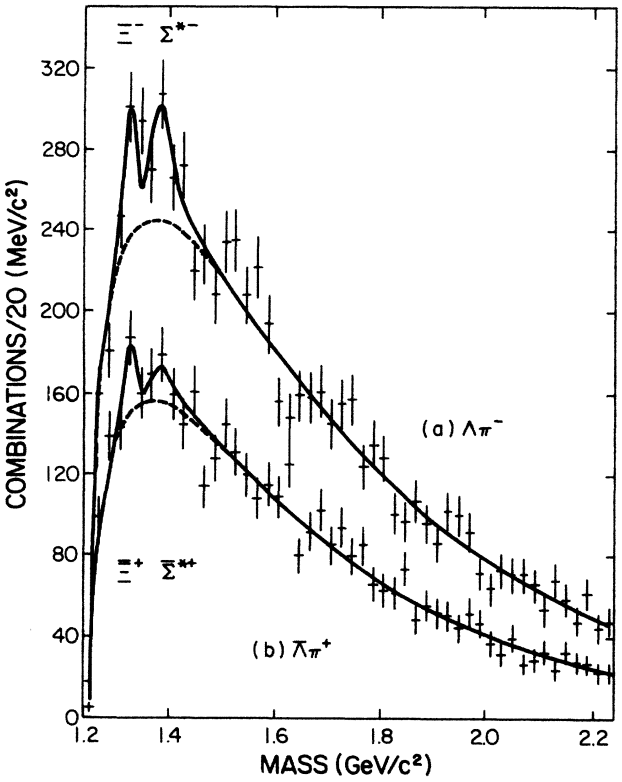

FIG. 14. Mass spectra for (a) $\Lambda\pi^{-}$ and (b) $\bar{\Lambda}\pi^{+}$.

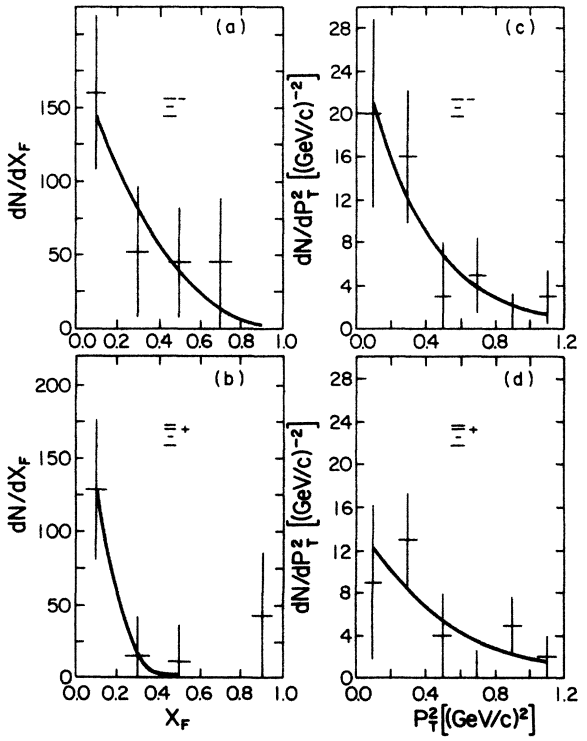

FIG. 13. The X_F distributions for (a) Ξ^{-}, (b) $\bar{\Xi}^{+}$; and the $P_T{}^2$ distributions for (c) Ξ^{-} and (d) $\bar{\Xi}^{+}$.

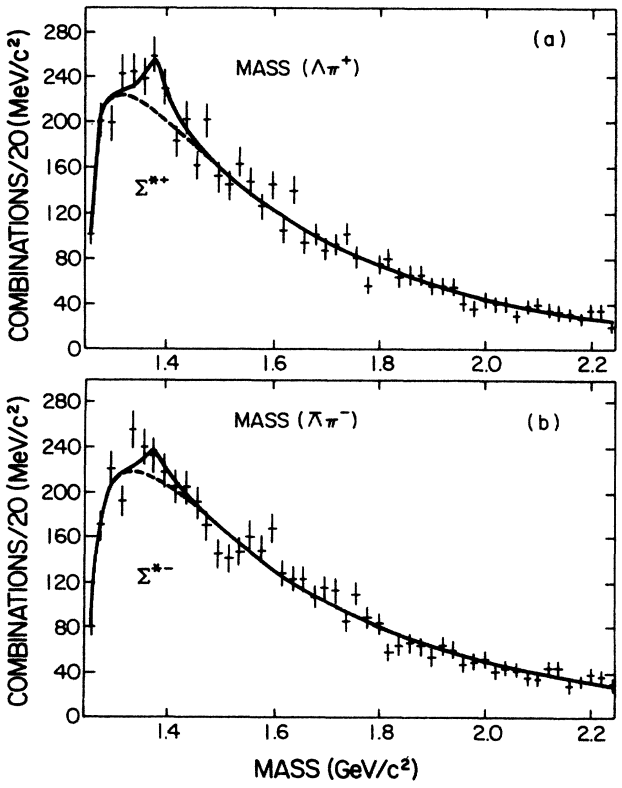

FIG. 15. Mass spectra for (a) $\Lambda\pi^{+}$ and (b) $\bar{\Lambda}\pi^{-}$.

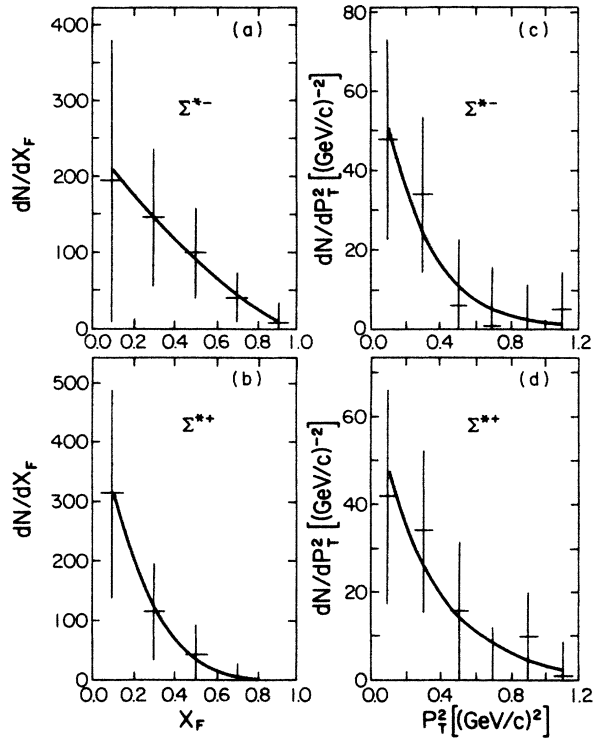

FIG. 16. The X_F distribution for (a) Σ^{*-}, (b) Σ^{*+}; and the $P_T{}^2$ distributions for (c) Σ^{*-} and (d) Σ^{*+}.

particles with the initial valence beam quark, we conclude that valence quarks play a significant role in strange-particle production.

In Table IV we summarize the fits to X_F distributions from other π^- beam experiments whose comparison with the predictions are found elsewhere.[2] Recent E580 results[9] for $K^*(892)$ from $K_S^0K_S^0X$ data found $n=0.64\pm0.12$ for K^{*-}, 2.76 ± 0.32 for K^{*+}, and $R(K^{*+}/K^{*-})=0.89\pm0.19$ with $n=2.24\pm0.34$. $\bar{K}^{*0}$ and K^{*0} produced by 175 GeV π^- on beryllium[12] gave $n=0.69\pm0.10$ $(0.1\leq X_F\leq 0.9)$ and 0.59 ± 0.13 $(0.3\leq X_F\leq 0.9)$ for K^{*0}, 1.82 ± 0.27 $(0.1\leq X_F\leq 0.9)$ and $1.47\pm0.51(0.3\leq X_F\leq 0.9)$ for $\bar{K}^{*0}$, and $R(\bar{K}^{*0}/K^{*0})=0.86\pm0.08$ with $n=1.11\pm0.27$, consistent within errors to our $R(K^{*+}/K^{*-})$ at $X_F\sim 0$. K^+ and K^- production[13] gave, for $0.12<X_F<0.5$, $n=2.06\pm0.25$ for $\pi^-\to K^-$ and, for $0.12<X_F<1.0$, $n=2.85\pm0.22$ for $\pi^-\to K^+$ at 175 GeV/c and similarly 1.84 ± 0.30 and 1.76 ± 0.10 at 100 GeV/c. The inclusive spectra from 200-GeV/c π^--beryllium interactions[14] at $P_T=0$ gave $n=0.262\pm0.013$ for K_S^0, and 3.01 ± 0.09 and 3.05 ± 0.11 for Λ and $\bar{\Lambda}$. The K_S^0 and $K^\pm$ distributions were intermediate between those of K^{*+} and K^{*-} values, as expected for significant resonance decay. Our K_S^0 results are consistent with the 100-GeV/c charged-kaon data and the 175-GeV/c K^- data, but they are not consistent with the 175-GeV/c K^+ data. Further, our charged-K^* results are consistent with the 175-GeV/c neutral-K^* data.

Strange-baryon production[7] by a π^- beam from the $K_S^0\Lambda/K_S^0\bar{\Lambda}$ data gave $n=5.8\pm1.7$ for the combined $\Sigma^\pm(1385)+\bar{\Sigma}^\pm(1385)$ X_F distribution and 6.7 ± 0.3 for $\Xi^-(1321)+\bar{\Xi}^+(1321)$. QCR's predict $n=4$ for both fragmentation processes $K^-\to p$ and $\pi^-\to\Sigma^+(1385)$. From 100- and 175-GeV/c K^- data[15] $n=3.86\pm1.10$ for $0.2\leq X_F\leq 0.7$ and $0.3\leq P_T{}^2\leq 1.0$ (GeV/c)^2 in agreement with our $\Sigma^+(1385)$ value. Although QCR's[1] reasonably estimate the n values, our data exhibit systematic differences between various processes of the same class, which is presumably related to spin and flavor effects.

CROSS SECTIONS

The cross section is defined as $\sigma=SN_0/A'A$. N_0 is the number of observed events, A the spectrometer acceptance, A' a correction for inefficiencies not included in the acceptance, and S the microbarn equivalent of the experiment (i.e., the cross section for 1 event) calculated as $S=(N_tN_b)^{-1}=(32\,800\ \text{events}/\mu\text{b})^{-1}$, where N_t is the number of target particles $(6.02\times10^{23}/\text{g})\times[12.80(\text{scint})+0.548(\text{A1})+2.232(\text{tape})\text{g/cm}^2]$ or $93.79\times10^{23}/\text{cm}^2$, and N_b the effective (dead-time corrected) beam of 3.5×10^9. The experimental acceptance is a product of the probabilities that particles in an event will traverse the magnet and chambers (geometrical acceptance), the V^0 will decay within decay region, the trigger will operate as designed (trigger efficiency), and the software will properly reconstruct the event. Included in A' is a correction for the branching fractions for a given decay mode and other corrections not included in A.

The trigger for V^0 events was estimated to be ~4 times

TABLE III. Fits to $(1-X_F)^n$ distributions, this experiment.

Reaction	X_F	n (expt)	χ^2/DF	n (pred.)[a]
$\pi^-\to K_S{}^0$	0.2–0.8	1.7±0.1	10/13	1 or 3
$\pi^-\to K^{*-}$	0.2–1.0	0.9±0.2	3/2	1
$\pi^-\to K^{*+}$	0.2–1.0	1.9±0.4	1/2	3
$\pi^-\to\Lambda$	0.2–0.8	2.0±0.1	7/11	2
$\pi^-\to\bar{\Lambda}$	0.2–0.8	2.0±0.1	12/11	2
$\pi^-\to\Sigma^{*-}$	0.0–1.0	1.4±0.4	0.04/3	2
$\pi^-\to\Sigma^{*+}$	0.0–0.8	3.8±2.2	0.07/2	4
$\pi^-\to\Xi^-$	0.0–1.0	2.2±2.0	1/2	2
$\pi^-\to\bar{\Xi}^+$	0.0–1.0	8.4±9.0	1/2	4

[a]From Ref. 2.

TABLE IV. Fits to $(1-X_F)^n$ distributions, other experiments. References 7 and 9 are the V^0V^0 data in E580.

Reaction	Reference	P_{lab} (GeV/c)	X_F	n (expt)
$\pi^-N\to K^{*-}$	9	200	0.0—1.0	0.64±0.12
$\pi^-N\to K^{*+}$	9	200	0.0—1.0	2.76±0.32
$\pi^-N\to\Sigma^{*\pm}$	7	200	0.0—1.0	5.8±1.7
$\pi^-N\to\Xi^{\pm}$	7	200	0.0—1.0	6.7±0.3
π^-Be$\to K^{*0}$	12	175	0.1—0.9	0.69±0.10
			0.3—0.9	0.59±0.13
π^-Be$\to\overline{K}^{*0}$	12	175	0.1—0.9	1.82±0.27
			0.3—0.9	1.47±0.51
$\pi^-p\to K^-$	13	175	0.1—0.5	2.06±0.25
$\pi^-p\to K^+$	13	175	0.1—1.0	2.85±0.22
$\pi^-p\to K^-$	13	100	0.1—0.5	1.84±0.30
$\pi^-p\to K^+$	13	100	0.1—1.0	1.76±0.10
π^-Be$\to K_S{}^0$	14	200	$P_T=0$	0.26±0.01
π^-Be$\to\Lambda$	14	200	$P_T=0$	3.01±0.09
π^-Be$\to\overline{\Lambda}$	14	200	$P_T=0$	3.05±0.11

lower than for the V^0V^0 events. Independently,[8] it was found that the V^0V^0 trigger efficiency was 0.40±0.04. The expected ratio of $K_S^0K_S^0$ to K_S^0 events from measured bubble-chamber cross sections[16] at 250 GeV/c using our estimated acceptances is 0.29±0.16, in agreement with our experimental value 0.255±0.003. Further, we compared the cross sections for the diffractive dissociation processes in the $K_S^0K_S^0$ and K_S^0 samples.

In Table V we summarize the calculated partial cross sections for our observed states assuming a 0.10±0.04 trigger efficiency, a 0.40±0.04 software efficiency, and the currently accepted branching fraction.[3] The geometrical and decay volume acceptances are estimated using Monte Carlo—generated events for a given reaction. The partial cross section is trigger dependent and represents the forward cross section for the given state, with only one V^0 in the final state and with low charge multiplicity. These cross sections are not inclusive cross sections because they do not contain events with more than one V^0 or high charge multiplicity. To estimate the total inclusive cross sections for states decaying into $V^0\pi\pm$ we must determine our cross-section normalization using those measured in a hydrogen bubble chamber[17] at 200 GeV/c: 3.74±0.24, 1.53±0.12, and 0.43±0.06 mb for K_S^0, Λ, and $\overline{\Lambda}$, respectively. We corrected for an additional observed pion by taking into account the relative acceptance V^0 and $V^0\pi$ for a given state. The total inclusive cross sections are given in Table V.

Other inclusive strange resonance production data in high-energy πN interactions are limited. A summary of the energy dependence for the K^* cross section is found elsewhere.[11] In 175-GeV/c π^--beryllium interactions,[12] the inclusive cross section $(0.0\le X_F\le 1.0)$ is 610±20±90 and 380±20±60 μb for $K^{*0}(892)$ and $\overline{K}^{*0}(892)$, respectively. We conclude that there is no difference in π^- production of neutral and charged $K^*(892)$. For π^+p interactions[11] at 147 GeV/c the cross sections are 1300±200 μb and 700±200 μb for K^{*+} and K^{*-}, respectively, and are similarly 1500±300 and 1200±300 μb for pp interactions.

A summary of the energy dependence of the Ξ and of the $\Sigma^*(1385)$ cross section is found elsewhere.[18] The total inclusive cross sections for the $K_S^0\Lambda/K_S^0\overline{\Lambda}$ sample[7] are 41±4 and 23±8 μb for $(\Xi^-+\overline{\Xi}^+)$ and $[\Sigma^{*\pm}(1385)+\overline{\Sigma}^{*\pm}(1385)]$ production, respectively. In

TABLE V. The cross sections for observed states.

State	Observed events	Partial cross section[a] (μb)	Total cross section[b] (μb)
$K_S{}^0$	25 565±160	109.1±45.0	
Λ	3 999±63	22.6±9.3	
$\overline{\Lambda}$	3 041±55	17.2±7.1	
$K^{*-}(892)$	2 706±313	32.2±13.8	1103.5±168.8
$K^{*+}(892)$	1 813±309	21.6±9.6	739.4±146.0
$\Sigma^-(1385)$	219±50	1.6±0.7	105.2±30.1
$\Sigma^+(1385)$	154±46	1.1±0.6	74.0±25.5
$\Xi^-(1321)$	48±10	0.5±0.2	35.1±9.5
$\Xi^+(1321)$	33±10	0.4±0.2	8.9±3.0

[a]Based on forward sensitivity $S=(N_tN_b)^{-1}=(32\,800\ \text{events}/\mu\text{b})^{-1}$ with associated low charged multiplicity.

[b]Based on average normalization to the bubble-chamber data (Ref. 17).

147-GeV/c π^+p interactions,[11] the inclusive $\Sigma^{*+}(1385)$ cross section is 290 ± 70 μb and $\Sigma^{*-}(1385)<100$ μb. At the CERN ISR for $X_F>0.4$ the cross sections were measured as[19] 250, 40, and 9 μb for $\Sigma^+(1385)$, $\Sigma^-(1385)$, and $\Xi^-(1320)$, respectively. However, they studied the proton fragmentation region, while we observe the forward hemisphere which includes the central and π^- fragmentation regions.

Compared with other measurements our $K^{*\pm}$ cross sections show an increase with beam energy and are consistent with other data. The Ξ^- cross section is consistent with low-energy results assuming a logarithmic energy dependence. For $\Sigma^{*\pm}$, the low-energy $\pi^\pm$ cross sections increase with beam energy. Assuming similar trends as the π^+ and p data show at higher energies, we expect the $\Sigma^{*\pm}$ production cross sections to be ~300 μb at 200 GeV/c. Thus, our $\Sigma^{*\pm}$ cross sections may be systematically underestimated, or the π^- energy dependence is weaker than for other beams.

DIFFRACTIVE PRODUCTION

Diffractive dissociation, widely observed in hadroproduction, has been little studied for flavor dependence.[20] The diffractive π^- fragmentation[6] into $K^0_SK^0_S\pi^+\pi^-\pi^-$ (1.6 ± 0.8 μb) and $K^0_SK^0_S\pi^-$ (3.4 ± 1.0 μb) give a cross-section ratio of 0.40 ± 0.13, in agreement with 0.36 expected assuming the asymptotic topological cross section $\sigma=C/N^2$, where C is a constant and N is the charged plus neutral multiplicity.

Using these results, we expect diffractive dissociation $\pi^-\to K^0K^-\pi^+\pi^-$ and $\bar{K}^0K^+\pi^-\pi^-$ cross sections of ~8–10 μb. To test this hypothesis we study the reaction $\pi^-\to K^0_S\pi^+\pi^-\pi^-$ assuming that one pion is an unidentified kaon. Using 4255 K^0_S events with one positive and two negative primary tracks we isolate the diffractive component in the recoiling mass squared (MM^2), shown in Fig. 17(a), and interpret the peak at 1 (GeV/c^2)^2 as the recoiling target nucleon.

For exclusive reactions considerable effort is made to eliminate or correct for nondiffractive background. The shaded histogram in Fig. 17(a) shows the mass distribution recoiling against $K^0_S\pi^+\pi^+\pi^-$, where no similar low-mass peak is expected or evident, since net positive charge final states cannot be produced diffractively. To estimate the nondiffractive background in $K^0_S\pi^+\pi^-\pi^-$ we fit a polynomial to the shaded histogram and normalize it to the unshaded histogram [$203.5\le MM^2\le273.5$ (GeV/c^2)^2] and obtain the distribution shown in Fig. 17(b).

To correct for diffractive events with an unseen π^0, we assume that removing a π^0 from $K^0_S\pi^+\pi^-\pi^-\pi^0$ is equivalant to removing the π^+ from $K^0_S\pi^+\pi^-\pi^-$. We therefore use the $K^0_S\pi^+\pi^-\pi^-$ events with $MM^2<18.5$ (GeV/c^2)^2, throw out the π^+, calculate the $K^0_S\pi^-\pi^-$ MM^2 which we plot in Fig. 17(c). Normalizing this histogram for $23.5\le MM^2\le273.5$ (GeV/c^2)^2 to that in Fig. 17(b) and subtracting, we obtain Fig. 17(d). The low-mass peak FWHM is consistent with 14 (GeV/c^2)^2, the calculated spectrometer MM^2 resolution. We assume that the 304 ± 30 events with $MM^2<18.5$ (GeV/c^2)^2 are mostly single, with some double, diffractive events. To check

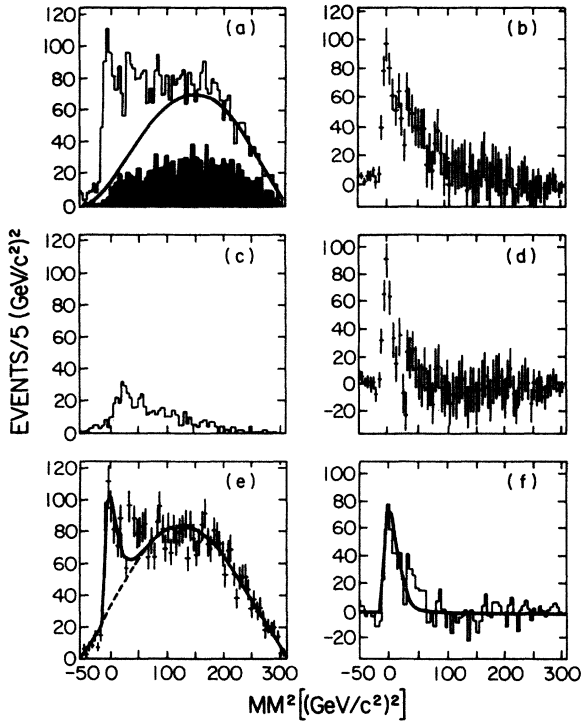

FIG. 17. The analysis of diffraction production $\pi^-\to K^0_S\pi^+\pi^-\pi^-$ explained in the text.

this result, we fit the logarithmic-normal distribution plus polynomial background to the $K^0_S\pi^+\pi^-\pi^-$ distribution in Fig. 17(e). In Fig. 17(f) we plot the fitted logarithmic-normal distribution (solid curve) (Ref. 21) after background subtraction and obtain 300^{+38}_{-22} $K^0_S\pi^+\pi^-\pi^-$ diffractive events with $MM^2<18.5$ (GeV/c^2)^2 in agreement with the first method.

To obtain the cross section we normalize our K^0_S sample to the 1.41 ± 0.28 mb bubble-chamber forward-inclusive K^0_S production cross section.[16] Comparing the geometrical decay volume acceptances and trigger efficiencies for diffractive and all K^0_S events, we obtain $\pi^-\to K^0K^-\pi^+\pi^-$ and $\bar{K}^0K^+\pi^-\pi^-$, single-diffractive cross sections of 11.2 ± 5.9 μb per channel, assuming that each channel contributes equally, in agreement with the expected value.

SUMMARY

We studied the strange-resonance production in π^-N interactions at 200 GeV/c with only one K^0_S Λ, or $\bar{\Lambda}$ in the final state. For $K^*(892)$ production we find no difference between charged (K^{*-},K^{*+}) and neutral (K^{*0}, $\bar{K}^{*0}$), but individually each is systematically produced more forward than QCR's predict, indicating that valence quarks play an important role in strange-particle production. A third of the K^0_S came from K^* decay. Strange-baryon production is well predicted by QCR's. $\pi^-\to K^0K^-\pi^+\pi^-$ and $\bar{K}^0K^+\pi^-\pi^-$ diffractive dissociation cross sections are consistent with fragmentation estimates.

ACKNOWLEDGMENTS

We appreciate the assistance of R. Cantel and S. Hansen in preparing and running this experiment. Our work was supported by the Department of Energy (Arizona, Fermilab, Florida State, Tufts) and the National Science Foundation (Arizona, Notre Dame, Vanderbilt, Virginia Tech).

---

[a]Present address: Notre Dame University, Notre Dame, IN 46556.
[b]Present address: Lab. Nazionali, Frascatti (Roma), Italy.
[c]Present address: Nanking University, People's Republic of China.
[d]Present address: Burr-Brown Research, Tucson, AZ 85706.
[e]Present address: HEPL, Stanford, CA 94305.
[f]Present address: Planning Systems, Panama City, FL 32401.
[g]Present address: AT&T Laboratories, West Longbranch, NJ 07764.
[h]Present address: AT&T Laboratories, Naperville, IL 60566.
[i]Present address: American Dade, Costa Mesa, CA 92660.
[j]Present address: Motorola, Tucson, AZ 85721.
[k]Present address: 61 Batten Hall, Worchester, United Kingdom.

[1]P. D. B. Collins and A. D. Martin, Rep. Prog. Phys. **45**, 335 (1983); K. Fialkowski and W. Kittel, *ibid.* **46**, 1283 (1983).
[2]J. F. Gunion, Phys. Lett. **88B**, 150 (1979).
[3]Particle Data Group, C. G. Wohl *et al.*, Rev. Mod. Phys. **56**, S1 (1984).
[4]A. Kernan and G. VanDalen, Phys. Rep. **106**, 298 (1984).
[5]T. Y. Chen *et al.*, Phys. Rev. D **28**, 2304 (1983).
[6]C. C. Chang *et al.*, Phys. Rev. D **29**, 1888 (1984).
[7]H. C. Fenker *et al.*, Phys. Rev. D **30**, 872 (1984).
[8]E. G. H. Williams *et al.*, Phys. Rev. D **30**, 877 (1984).
[9]A. Napier *et al.*, Phys. Lett. **149B**, 514 (1984).
[10]S. Torres, Ph.D. thesis, Virginia Polytechnic Institute, 1984.
[11]D. Brick *et al.*, Phys. Rev. D **25**, 2248 (1982).
[12]R. Bailey *et al.*, Z. Phys. C **24**, 111 (1984).
[13]A. E. Brenner *et al.*, Phys. Rev. D **26**, 1497 (1982).
[14]R. T. Edwards *et al.*, Phys. Rev. D **18**, 76 (1978).
[15]D. Cutts *et al.*, Phys. Rev. Lett. **43**, 319 (1979).
[16]D. Bogert *et al.*, Phys. Rev. D **16**, 2098 (1977).
[17]N. N. Biswas *et al.*, Nucl. Phys. **B167**, 41 (1980).
[18]P. V. Chliapnikov, in *Proceedings of the XI International Symposium on Multiparticle Dynamics, Bruges, Belgium, 1980,* edited by E. De Wolf and F. Verbeure (University of Antwerp, Belgium, 1980).
[19]S. Erhan *et al.*, Phys. Lett. **85B** 447 (1979).
[20]G. Alberi and G. Goggi, Phys. Rep. **74**, 2 (1981); K. Goulianos, *ibid.* **101**, 174 (1983).
[21]W. T. Eadie, D. Drijard, F. E. James, M. Roos, and B. Sadoulet, *Statistical Methods in Experimental Physics* (North-Holland, Amsterdam, 1973).